Supplementary Information

Title: Underwater dielectric elastomer actuators with large bending deformation for soft robots

Authors:

Chiho Murata[1], Takumi Shibuya[1], Naoki Uemura[2], Kengo Kusama[1], Daisuke Nakane[2], Masahiro Shimizu[3], and Jun Shintake[1]*

Affiliations:

[1]Department of Mechanical and Intelligent Systems Engineering, The University of Electro-Communications, 1-5-1 Chofugaoka, Chofu, Tokyo 182-8585, Japan

[2]Department of Engineering Science, The University of Electro-Communications, 1-5-1 Chofugaoka, Chofu, Tokyo 182-8585, Japan

[3]Department of Bioscience, Nagahama Institute of Bio-Science and Technology, 1266 Tamuracho, Nagahama, Shiga 526-0829, Japan

E-mail: shintake@uec.ac.jp

Supplementary movie legends:

Movie 1. Bending deformation of the actuator

Movie 2. Mechanoluminescence of the electrically-driven biohybrid actuator containing *Pyrocystis lunula* (repeated sequence)

Movie 3. Demonstration of a soft gripper for manipulating a live jellyfish

This PDF file includes:

Supplementary Note 1. Actuator model

Supplementary Figure 1. Schematic illustrations of the actuator model

Supplementary Figure 2. Dimensions of the actuator components

Supplementary Table 1. Bending angle and actuation speed in previous studies of underwater robots based on DEAs

Supplementary Table 2. Parameters used in the analytical model of the actuator

Supplementary Table 1. Bending angle and actuation speed in previous studies of underwater robots based on DEAs.

Reference	Bending angle [º]	Actuation speed [º/s]	Note
Li et al. [1]	10.2	~102.0	Actuation speed is estimated from the driving frequency.
Cheng et al. [2]	N/A	N/A	
Christianson et al. [3]	~34.0	~13.6	Bending angle and actuation speed are estimated from the tip deflection and the driving frequency.
Kusama et al. [4]	21.8	~21.8	Actuation speed is estimated from the driving frequency.
Li et al. [5]	6.3	~6.3	Actuation speed is estimated from the driving frequency.
Wang et al. [6]	48.0	~74.0	Actuation speed is estimated from the driving frequency.
Shintake et al. [7]	~12.6	~12.6	Bending angle and actuation speed are estimated from the tip deflection and the driving frequency.
Wang et al. [8]	40.0	~80.0	Actuation speed is estimated from the driving frequency.
Zhang et al. [9]	5.0	~50.0	Actuation speed is estimated from the driving frequency.

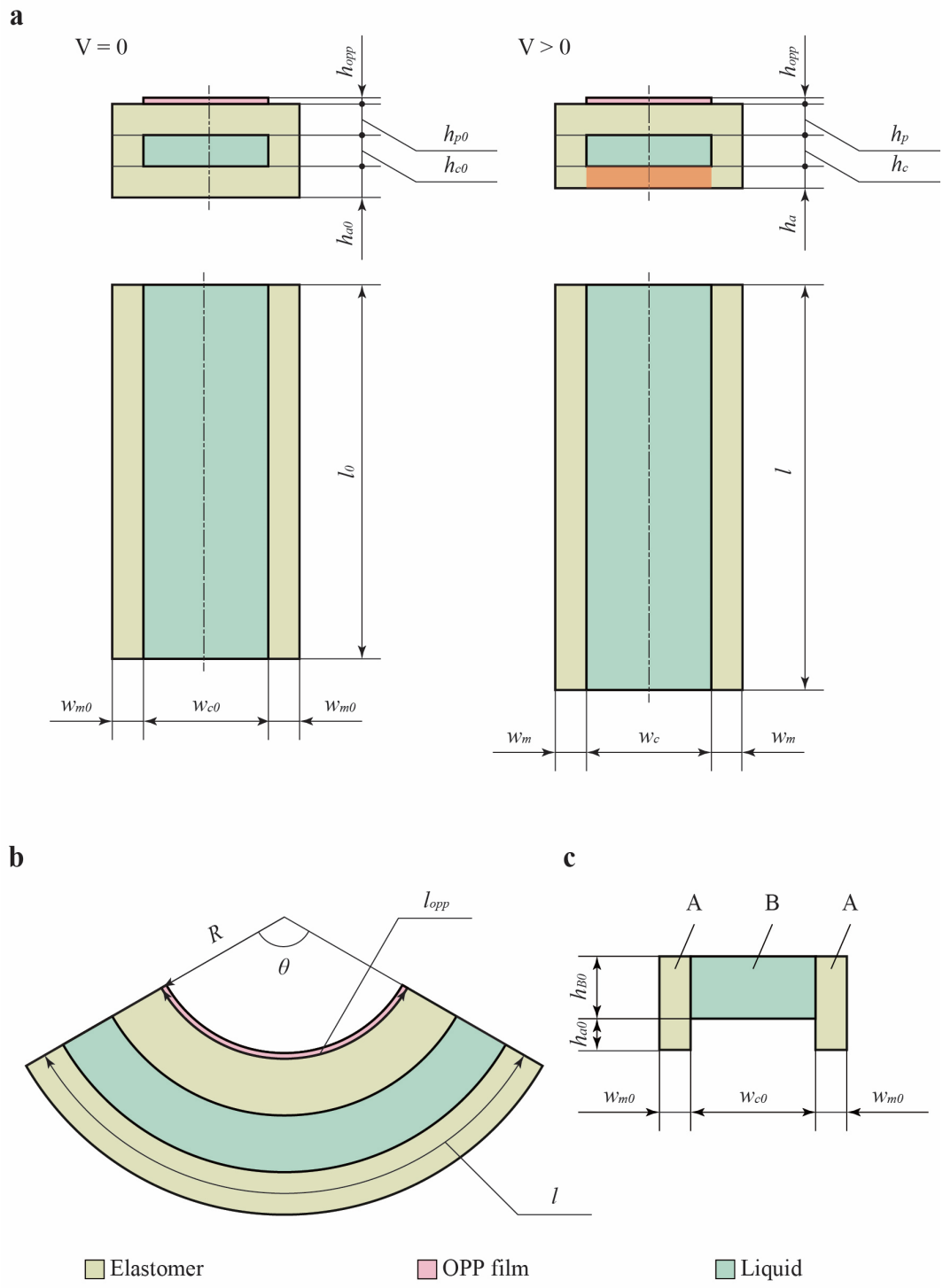

Supplementary Figure 1. Schematic illustrations of the actuator model. (a) Longitudinal view and cross-sectional view of the actuator. (b) Side view of the actuator in the bent state. (c) Cross-sectional view of the actuator structure considered in the model.

Supplementary Note 1. Actuator model

To predict the behavior of the proposed actuator and to facilitate its design, an analytical model was developed. The bending angle was determined by minimizing the total potential energy,

following the approach of previous studies [10,11]. The total potential energy considered in the model consists of strain energy, electrostatic energy, and bending energy.

As shown in Supplementary Figure 1a, the structure consists of an OPP film, a top elastomer layer, an intermediate elastomer layer containing the chamber filled with water, and a bottom elastomer layer. When a voltage is applied to the actuator, the bottom layer is compressed in the thickness direction and expands in the longitudinal direction. On the other hand, the OPP film is non-stretchable and restricts the elongation. Due to the presence of the OPP film, the deformation in the thickness direction of the top elastomer layer is considered negligible. Therefore, in the model, the active layer is defined as the domain of the bottom elastomer layer sandwiched between the chamber and the surrounding water, as indicated by the orange region in Supplementary Figure 1a. The other parts are considered passive layers. Let l_0 be the initial length along the longitudinal direction at the center of the bottom elastomer layer in the thickness direction, and l be its length after voltage application. Defining the stretch ratio in the longitudinal direction as λ_1, the deformation of the bottom elastomer layer can be expressed as follows:

$$l = l_0 \lambda_1 \tag{1}$$

Since the elastomer is incompressible and its volume remains constant before and after deformation, the stretch ratios in the width and thickness directions, denoted as λ_2 and λ_3, respectively, satisfy the following relationship:

$$\lambda_1 \lambda_2 \lambda_3 = 1 \tag{2}$$

The actuator is constrained from bending deformation and elongation in the width direction by the PET frames, so $\lambda_2 = 1$. From Equation (2), each stretch ratio is given as follows.

$$\lambda_1 = \frac{l}{l_0}, \qquad \lambda_2 = 1, \qquad \lambda_3 = \frac{1}{\lambda_1 \lambda_2} = \frac{1}{\lambda_1} \tag{3}$$

Assuming that the actuator bends into an arc shape as shown in Supplementary Figure 1b, the length of the bottom elastomer layer can be expressed using the radius of curvature R from the center of the arc to the OPP film and the central angle θ as follows:

$$
\begin{aligned}
l &= \left(R + h_p + h_c + \frac{h_a}{2}\right)\theta \\
&= l_{opp} + \left(h_{p0} + h_{c0} + \frac{h_{a0}\lambda_3}{2}\right)\theta \\
&= l_{opp} + \left(h_{p0} + h_{c0} + \frac{1}{2}h_{a0}\frac{l_0}{l}\right)\theta \\
\leftrightarrow\ & l^2 - \{l_{opp} + (h_{p0} + h_{c0})\theta\}l - \frac{1}{2}h_{a0}l_0\theta = 0
\end{aligned} \tag{4}
$$

Here, l_{opp} represents the length of the OPP film, which is used as the reference length during deformation since it is non-extensible. Although R is defined to the upper surface of the OPP film, the thickness of the OPP film h_{opp} is neglected because it is much smaller than the thickness of the elastomer layers. The variables h_{p0}, h_{c0}, and h_{a0} denote the initial thicknesses of the top elastomer layer, intermediate layer, and active layer, respectively, before voltage application, while h_p, h_c, and h_a represent their thicknesses after voltage application. However, as the model assumes that only the active layer is subjected to electrostatic compression, the thickness of the top elastomer layer and intermediate layer are considered to be constant.

In the model, the strain energy is considered only in the active layer (the orange region in Supplementary Figure 1a), which is the region subjected to electrostatic compression. This corresponds to the chamber region in the longitudinal direction of the actuator. The Yeoh hyperelastic model ([12]) is used to calculate the strain energy. The strain energy density function is expressed as follows:

$$
W = \sum_{i=1}^{3} c_i (I_1 - 3)^i \tag{5}
$$

where c_i are material constants, and $I_1 = \lambda_1^2 + \lambda_2^2 + \lambda_3^2$. Let w_c be the width of the chamber region. From Equation (5), the strain energy can be expressed as follows:

$$
\begin{aligned}
U_{strain} &= vol \cdot W(\theta) \\
&= l_0 w_{c0} h_{a0} \sum_{i=1}^{3} c_i (\lambda_1^2 + \lambda_2^2 + \lambda_3^2 - 3)^i
\end{aligned} \tag{6}
$$

The electrostatic energy at an applied voltage V is defined as follows:

$$\begin{aligned} U_{electric} &= -\frac{1}{2}CV^2 \\ &= -\frac{1}{2}\varepsilon_0\epsilon_r\frac{lw_c}{h_a}V^2 \\ &= -\frac{1}{2}\varepsilon_0\epsilon_r\frac{l_0\lambda_1 w_{c0}\lambda_2}{h_{a0}\lambda_3}V^2 \\ &= -\frac{1}{2}\varepsilon_0\epsilon_r\frac{l_0 w_{c0}{\lambda_1}^2}{h_{a0}}V^2 \end{aligned} \quad (7)$$

where C is the capacitance, ε_0 is the permittivity of free space, and ε_r is the relative permittivity of the elastomer. The electrostatic energy is considered negative because it represents the work done on the actuator by the external source.

In the model, the bending energy is considered for the passive layers, namely the top elastomer layer, the intermediate elastomer layer filled with water, and the inactive domain of the bottom elastomer layer. As the chamber is filled with water and the volume of water remains constant and incompressible, the chamber section is also assumed to behave as an elastomer. To calculate the bending energy, the second moment of area was determined. For this purpose, the cross-section was modeled as a U-shape, as shown in Supplementary Figure 1c, which corresponds to the cross-section without the active domain. The cross-section is divided into three regions: two regions of type A and one region of type B. The area A_A, centroid in the thickness direction G_A, and second moment of area I_A for region A are defined as follows:

$$h_{B0} = h_{p0} + h_{c0}$$

$$A_A = w_{m0} \times (h_{B0} + h_{a0})$$

$$G_A = \frac{1}{2}(h_{B0} + h_{a0}) \quad (8)$$

$$I_A = \frac{w_{m0} \times (h_{B0} + h_{a0})^3}{12} \quad (9)$$

The area A_B, centroid in the thickness direction G_B, and second moment of area I_B for region B are defined as follows:

$$A_B = w_{c0} \times h_{B0}$$

$$G_B = \frac{1}{2} h_{B0} \tag{10}$$

$$I_B = \frac{w_{c0} \times {h_{B0}}^3}{12} \tag{11}$$

The centroid in the thickness direction G_U for the entire U-shaped structure, including both regions A and B, was determined based on the moment balance. The total area A_U is the sum of the areas of A and B.

$$A_U = 2A_A + A_B$$

$$A_U \times G_U = 2A_A \times G_A + A_B \times G_B$$

$$G_U = \frac{2A_S \times G_A + A_B \times G_B}{A_U} \tag{12}$$

Using the parallel axis theorem, the second moments of area of regions A and B around their respective centroids, G_A and G_B, were transformed to the centroidal axis of the U-shaped structure G_U. Based on Equations (8), (9), (10), and (11), the following expressions are obtained:

$$I'_A = I_A + A_A \times (G_A - G_U)^2 \tag{13}$$

$$I'_B = I_B + A_s \times (G_U - G_B)^2 \tag{14}$$

Based on Equations (13) and (14), the second moment of area for the U-shaped cross-section, I_U, is given by the following expression:

$$I_U = 2I'_A + I'_B \tag{15}$$

From the second moment of area calculated in Equation (15), the bending energy can be calculated as follows:

$$U_{bend} = \frac{1}{2}K\theta^2 = \frac{1}{2}\frac{YI_U}{l}\theta^2 \quad (16)$$

where K is the rotational spring constant, and Y is the Young's modulus of the elastomer. The total potential energy of the actuator is the sum of Equations (6), (7), and (16):

$$U_{total} = U_{strain} + U_{electric} + U_{bend} \quad (17)$$

Minimizing Equation (17) is equivalent to solving the following equation:

$$\frac{\partial U_{total}}{\partial \theta} = 0 \quad (18)$$

Accordingly, the bending angle of the actuator with respect to the applied voltage can be determined. Table 2 summarizes the values of the parameters used for the design and prediction of the actual device.

Supplementary Table 2. Parameters used in the analytical model of the actuator.

Dimensions	
OPP film thickness h_{opp}	20 μm
OPP film length l_{opp}	60 mm
Top elastomer layer thickness h_{p0}	0.5 mm
Intermediate elastomer layer thickness h_{c0}	0.5 mm
Chamber width w_{c0}	20 mm
Margin width w_{m0}	5 mm
Bottom elastomer layer thickness h_{a0}	0.5 mm
Material property	
Elastomer	
Dielectric constant ε_r	3.21[*1]
Material constant C_1	0.014070 MPa[*2]
Material constant C_2	-1.8493×10^{-4} MPa[*2]
Material constant C_3	4.042×10^{-6} MPa[*2]
Young's modulus Y	0.26 MPa[*3]
Other parameters	
Permittivity of free space ε_0	8.85×10^{-12} F/m

[*1] Dielectric constant of VHB4905 at 1 kHz, taken from Ref. [13].
[*2] Yeoh model material constants of VHB4905, taken from Ref. [14].
[*3] Young's modulus of VHB4905, taken from Ref. [15].

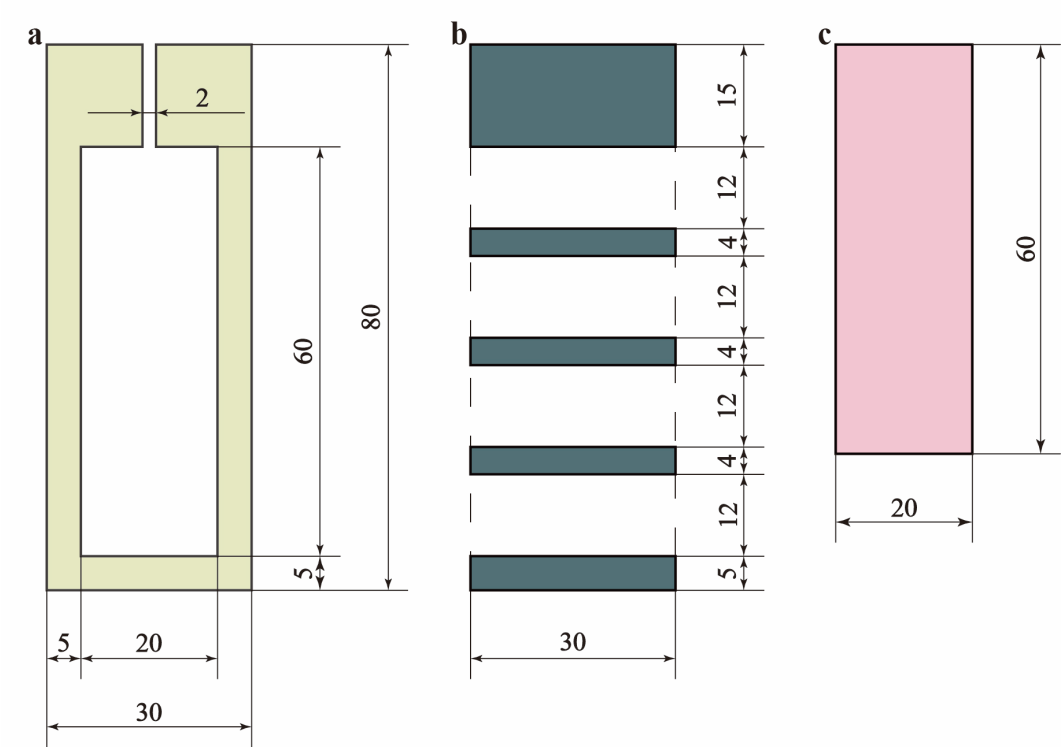

Supplementary Figure 2. Dimensions of the actuator components. (a) Intermediate elastomer layer defining the chamber and tube insertion region. (b) PET frame used to reinforce the actuator and constrain lateral deformation. (c) OPP film used as a flexible but non-stretchable constraint layer.

Supplementary References

1. Li, T. *et al.* Fast-moving soft electronic fish. *Sci. Adv.* **3**, 1–7 (2017).
2. Cheng, T. *et al.* Untethered soft robotic jellyfish. *Smart Mater. Struct.* **28**, 015019 (2019).
3. Christianson, C. *et al.* Jellyfish-Inspired Soft Robot Driven by Fluid Electrode Dielectric Organic Robotic Actuators. *Front. Robot. AI* **6**, 1–11 (2019).
4. Kusama, K. *et al.* Electrically Driven, Bioluminescent Compliant Devices for Soft Robotics. *ACS Appl. Mater. Interfaces* **17**, 11248–11258 (2025).
5. Li, G. *et al.* Self-powered soft robot in the Mariana Trench. *Nature* **591**, 66–71 (2021).
6. Wang, R. *et al.* Soft Manta Ray Robot Based on Bilateral Bionic Muscle Actuator. *IEEE Robot. Autom. Lett.* **9**, 7723–7730 (2024).
7. Shintake, J., Cacucciolo, V., Shea, H. & Floreano, D. Soft Biomimetic Fish Robot Made of Dielectric Elastomer Actuators. *Soft Robot.* **5**, 466–474 (2018).
8. Wang, R. *et al.* Fast-Swimming Soft Robotic Fish Actuated by Bionic Muscle. *Soft Robot.* **11**, 845–856 (2024).
9. Zhang, C. W. *et al.* Manta Ray Inspired Soft Robot Fish with Tough Hydrogels as

Structural Elements. *ACS Appl. Mater. Interfaces* **14**, 52430–52439 (2022).

10. Shintake, J., Rosset, S., Schubert, B. E., Floreano, D. & Shea, H. R. A Foldable Antagonistic Actuator. *IEEE/ASME Trans. Mechatronics* **20**, 1997–2008 (2015).
11. Rosset, S., Araromi, O. A., Shintake, J. & Shea, H. R. Model and design of dielectric elastomer minimum energy structures. *Smart Mater. Struct.* **23**, 085021 (2014).
12. Yeoh, O. H. Some Forms of the Strain Energy Function for Rubber. *Rubber Chem. Technol.* **66**, 754–771 (1993).
13. 3M™ VHB™ Tape 4905 | 3M United States. https://www.3m.com/3M/en_US/p/d/b40065643/.
14. Wang, H., Cui, S. & Niu, F. Optimization and demonstration of two types of spring-roll dielectric elastomer actuators for minimally invasive surgery. *Front. Bioeng. Biotechnol.* **10**, 1016350 (2022).
15. Shintake, J., Matsuno, K., Kumegawa, S., Baba, K. & Takeuchi, H. Characterization of slide ring materials for dielectric elastomer actuators. *Smart Mater. Struct.* **31**, 025028 (2022).